JET PHYSICS AT HERA[†]

C. GLASMAN, for the H1 and ZEUS Collaborations
Departamento de Física Teórica C-XI, Facultad de Ciencias, Universidad Autónoma de Madrid, Cantoblanco, 28049 Madrid, Spain

Measurements of inclusive jet and dijet cross sections in photoproduction and deep inelastic scattering are presented. These measurements provide new tests of QCD, constrain the parton densities of the proton and the photon, and allow the search for new physics. Measurements of jet shapes are reported and used to test the differences between quark and gluon jets.

1 Introduction

The main sources of jets at HERA are deep inelastic scattering (DIS) and quasi-real photon-proton (γp) collisions (photoproduction). In DIS, a highly virtual photon ($Q^2 \gg 0$, where Q^2 is the virtuality of the exchanged photon) interacts with a parton from the proton. In hard photoproduction, a parton from the proton interacts with a quasi-real photon ($Q^2 \sim 0$) emitted by the electron beam. High-p_T jet production is sensitive to the parton densities in the proton, in particular the gluon density, and to the parton densities in the photon in γp interactions. The measurements of jet cross sections provide constraints on the proton and photon parton densities, constitute new tests of QCD and allow the search for new physics. The internal structure of a jet is another tool to investigate QCD predictions and is sensitive to the differences between quark and gluon jets. During $1994-1997$ HERA operated with positrons of energy $E_e = 27.5$ GeV colliding with protons of energy $E_p = 820$ GeV.

2 Photoproduction at HERA

In γp interactions, the cross section for the production of jets at leading order (LO) in perturbative QCD (pQCD) is given by two contributions, namely those of resolved and direct processes. In resolved processes, a parton from the photon interacts with a parton from the proton, whereas in direct processes, the photon interacts as a point-like particle with a parton from the proton. The two contributions to the jet production cross section can be written as

$$\sigma_{direct} = \int d\Omega \; f_{\gamma/e}(y) \; f_{j/p}(x_p, \mu_F^2) \; d\sigma(\gamma j \to \text{jet jet}) \tag{1}$$

and

$$\sigma_{resolved} = \int d\Omega \; f_{\gamma/e}(y) \; f_{i/\gamma}(x_\gamma, \mu_F^2) \; f_{j/p}(x_p, \mu_F^2) \; d\sigma(ij \to \text{jet jet}), \tag{2}$$

where $f_{\gamma/e}(y)$ is the flux of photons in the electron[a] which is usually estimated by the Weizsäcker-Williams approximation [1]; $f_{j/p}(x_p, \mu_F^2)$ are the parton densities in the proton (determined from e.g. global fits [2]), x_p is the fraction of the proton momentum taken by the parton and μ_F is the factorisation scale; and $d\sigma(\gamma(i)j \to \text{jet jet})$ is the subprocess cross section, calculable in pQCD. In the case of resolved processes, there is an additional ingredient: $f_{i/\gamma}(x_\gamma, \mu_F^2)$ are the parton densities in the photon, for which there is only partial information. The integral is performed over the phase space represented by "$d\Omega$".

[†]Talk given at the *XXXIVth Rencontres de Moriond*, QCD and High Energy Hadronic Interactions, Les Arcs, Savoie, France, March $20^{th} - 27^{th}$, 1999.

[a]The variable y is the fraction of the electron energy taken by the photon.

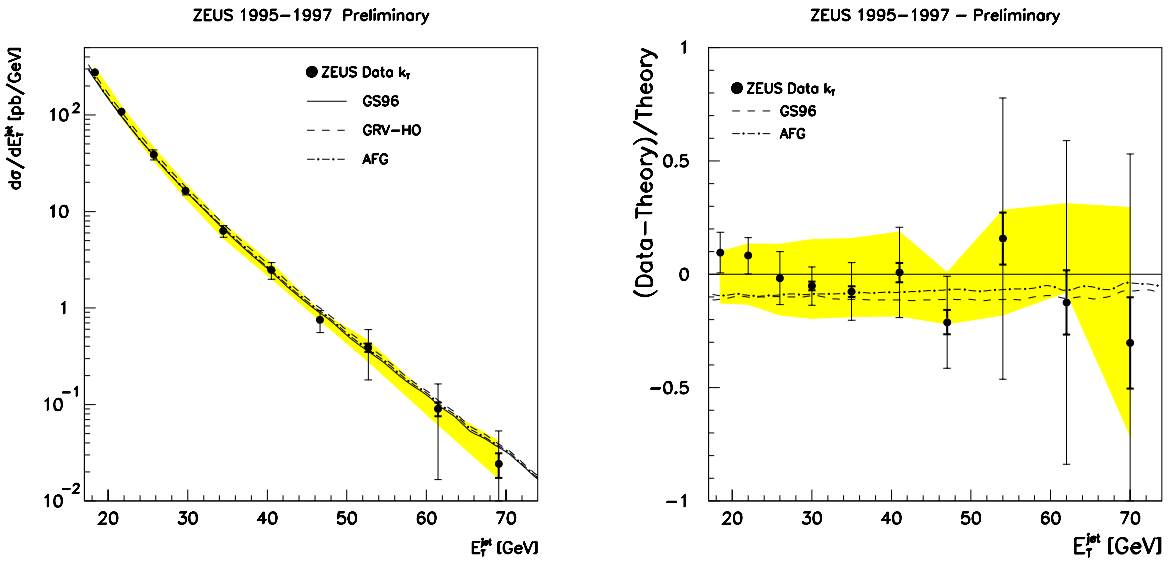

Figure 1: Measurement of the inclusive jet cross section $d\sigma/dE_T^{jet}$ in photoproduction. NLO QCD calculations are shown for comparison.

3 Inclusive jet cross sections in photoproduction

Inclusive jet cross sections in γp interactions are sensitive to the underlying parton dynamics and to the parton densities in the photon. To test the available parametrisations of the photon parton densities, the experimental and theoretical uncertainties must be reduced as much as possible. Two approaches have been followed to reduce the experimental uncertainties due to the so-called "underlying event" [3,4]: e.g. to decrease the cone radius in iterative cone jet algorithms [5,6] and/or to increase the jet transverse energy [3]. In this way, a region of phase space was found where the next-to-leading order (NLO) QCD calculations are able to describe the data [3]. However, the uncertainties in the calculations for the iterative cone algorithm are still sizeable. The use of the k_T cluster algorithm [7] reduces the theoretical uncertainties since it allows a transparent translation of the theoretical jet algorithm to the experimental set-up by avoiding the ambiguities related to the merging and overlapping of jets. In addition, a meaningful comparison between data and NNLO QCD calculations (when available) for the k_T cluster algorithm will be possible.

Inclusive jet cross sections have been measured [8] using the 1995 – 1997 ZEUS [9] data (which amounts to an integrated luminosity of $\mathcal{L} \sim 40$ pb^{-1}) as a function of the jet transverse energy (E_T^{jet}). The jets have been searched for with the k_T cluster algorithm. The measurements have been performed for jets of hadrons with E_T^{jet} between 17 and 74 GeV and jet pseudorapidity (η^{jet}) between -0.75 and 2.5, and are given for the kinematic region defined by $0.2 < y < 0.85$ and $Q^2 \leq 4$ GeV^2.

Figure 1 shows the measured $d\sigma/dE_T^{jet}$ (black dots). In figures 1 and 2, the systematic uncertainties not associated with the absolute energy scale of the jets have been added in quadrature to the statistical errors (thick error bars) and are shown as thin error bars. The shaded band represents the uncertainty on the energy scale of the jets. The data show a steep fall-off of four orders of magnitude in the measured range. The curves are NLO QCD calculations [10,11] using different parametrisations of the photon structure function: GS96 [12] (solid line), GRV-HO [13] (dashed line) and AFG [14] (dot-dashed line). The CTEQ4M [15] proton parton densities have been used in all cases. In the calculations shown here, the renormalisation and factorisation scales have been chosen equal to E_T^{jet} and α_s was calculated at 2-loops with $\Lambda^{(4)}_{\overline{MS}} = 296$ MeV. The NLO calculations give a reasonable description of the data. The right-hand side of figure 1 shows

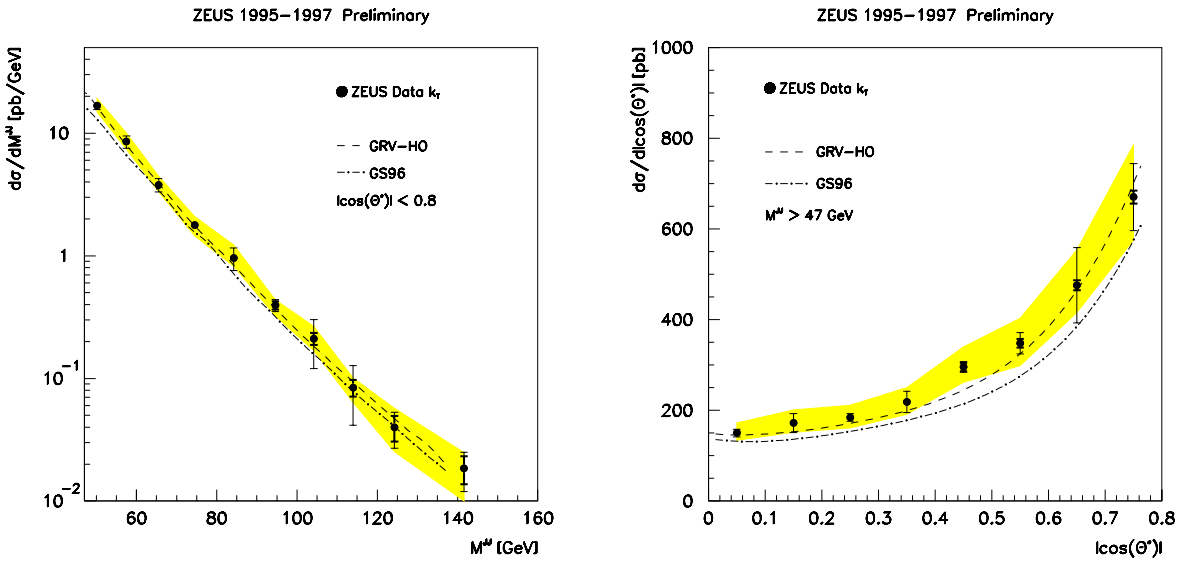

Figure 2: Measurement of the high-mass dijet cross sections $d\sigma/dM^{JJ}$ and $d\sigma/d|\cos\theta^*|$ in photoproduction. NLO QCD calculations are shown for comparison.

the fractional differences[b] between the measured $d\sigma/dE_T^{jet}$ and the NLO calculations. The NLO QCD calculations using the current knowledge of the photon structure are able to describe the data within the present experimental and theoretical uncertainties.

4 High-mass dijet cross sections in photoproduction

The dijet mass distribution M^{JJ} is sensitive to the presence of new particles or resonances that decay into two jets. The distribution of the angle between the jet-jet axis and the beam direction in the dijet centre-of-mass system ($\cos\theta^*$) reflects the underlying parton dynamics and is sensitive to the spin of the exchanged particle. New particles or resonances decaying into two jets may also be identified by deviations in the measured $|\cos\theta^*|$ distribution with respect to the QCD predictions.

High-mass dijet cross sections have been measured [16] using the 1995 – 1997 ZEUS data as a function of M^{JJ} and $|\cos\theta^*|$ in the kinematic region given by $0.2 < y < 0.85$ and $Q^2 \leq 4$ GeV^2. The measurements have been performed for $M^{JJ} > 47$ GeV and $|\cos\theta^*| < 0.8$ using the k_T cluster algorithm.

Figure 2 shows the measured $d\sigma/dM^{JJ}$ (left-hand side) and $d\sigma/d|\cos\theta^*|$ (right-hand side). The data show a steep fall-off in M^{JJ} of three orders of magnitude in the measured range. The measured $d\sigma/d|\cos\theta^*|$ rises as $|\cos\theta^*|$ increases. The NLO QCD calculations [10] give a reasonable description of the measured distributions. The predictions based on GRV-HO are closer in magnitude to the measured cross sections. No significant deviation between data and NLO calculations is observed in the measured range of M^{JJ} and $|\cos\theta^*|$.

5 Jet shapes in photoproduction

The internal structure of the jets has been studied by means of the differential and the integrated jet shape. The differential jet shape ($\rho(r)$) is defined as the averaged fraction of the jet transverse energy which lies in the annulus of width Δr at a distance r from the jet axis,

[b] The fractional differences are taken with respect to the NLO calculations based on GRV-HO.

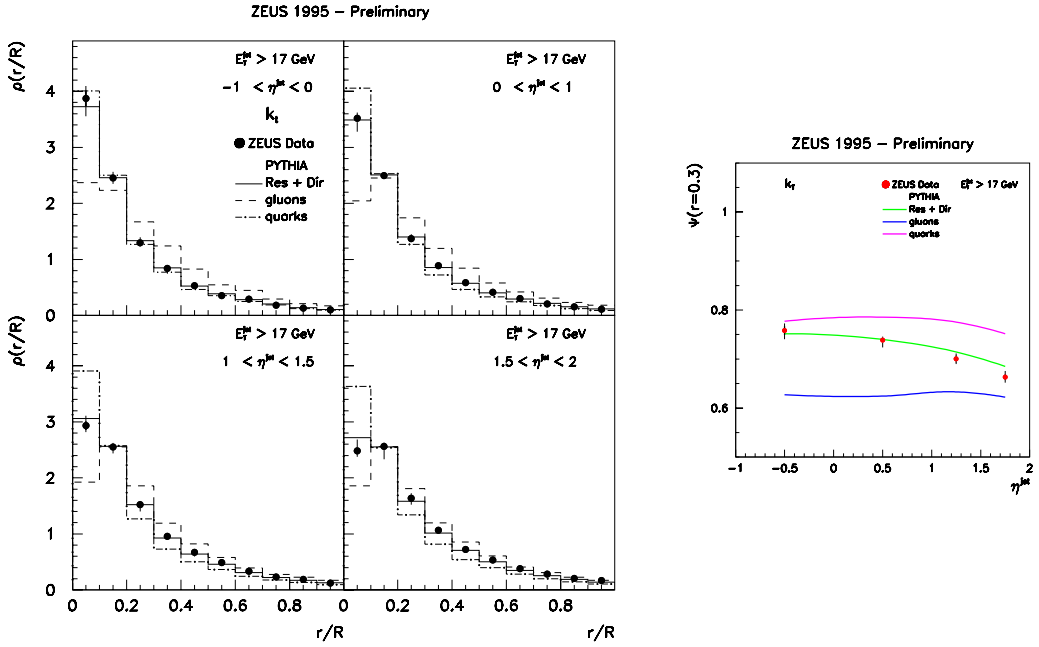

Figure 3: Measured differential (left-hand side) and integrated (right-hand side) jet shapes in photoproduction. Calculations from the leading-logarithm parton-shower Monte Carlo PYTHIA are shown for comparison.

$$\rho(r) = \frac{1}{N_{jets}\Delta r}\sum_{jets}\frac{E_T(r-\frac{\Delta r}{2}, r+\frac{\Delta r}{2})}{E_T(0,1)}, \tag{3}$$

where $E_T(r-\Delta r/2, r+\Delta r/2)$ is the transverse energy within the given annulus and N_{jets} is the total number of jets in the sample. The integrated jet shape ($\psi(r)$) is defined as

$$\psi(r) = \frac{1}{N_{jets}}\sum_{jets}\frac{E_T(0,r)}{E_T(0,1)}. \tag{4}$$

QCD predicts that at sufficiently high transverse energy, the jet shape is driven by gluon emission off the primary parton and therefore calculable in pQCD. Gluon jets are predicted to be broader than quark jets due to the gluon-gluon coupling strength being larger than that of the quark-gluon. At LO, a jet consists of only one parton and thus has no structure. NLO QCD calculations give the lowest non-trivial order contribution to the jet structure.

The differential and integrated jet shapes have been measured for jets defined with the k_T cluster algorithm and required to have $E_T^{jet} > 17$ GeV and $-1 < \eta^{jet} < 2$. The measurements have been performed using the 1995 ZEUS data ($\mathcal{L} \sim 6$ pb^{-1}) in the kinematic region given by $0.2 < y < 0.85$ and $Q^2 \leq 1$ GeV^2.

Figure 3 shows the measured differential jet shape $\rho(r)$ as a function of r in different regions of η^{jet} (left-hand side). The data (black dots) show that the jets become broader as η^{jet} increases. The solid histograms are the predictions of a leading-logarithm parton-shower Monte Carlo (MC) calculation using PYTHIA [17] for resolved and direct processes. The calculations, which include initial- and final-state QCD radiation, give a good description of the data. The dashed (dot-dashed) histograms are the predictions of PYTHIA for samples of gluon (quark) jets. The measured jets are dominated by quarks for $-1 < \eta^{jet} < 0$, and become increasingly more gluon-like as η^{jet} increases.

The quark and gluon content of the final-state jets has been studied in more detail by looking at the integrated jet shape for a fixed value of r ($r = 0.3$) as a function of η^{jet} (right-hand side of figure 3). The measured jet shape decreases with η^{jet}, i.e. the jets become broader as η^{jet} increases. Comparing the data to the model predictions for gluons (lower curve) and

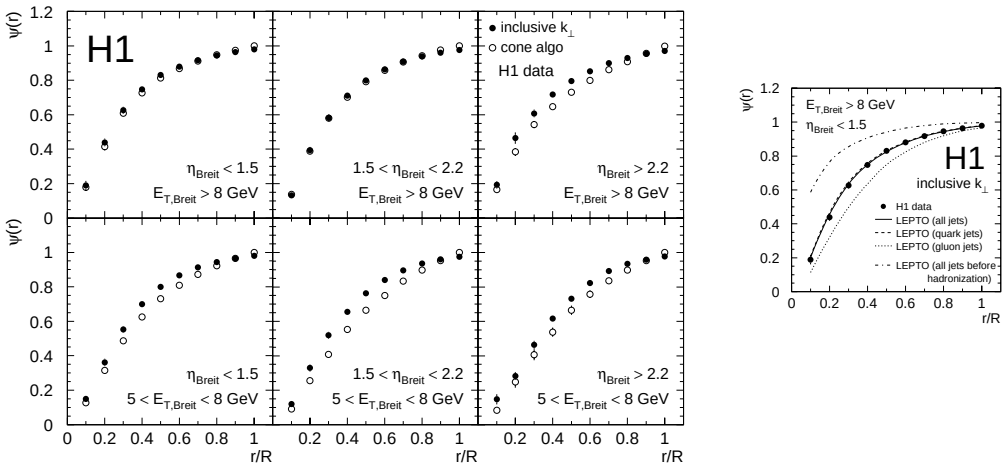

Figure 4: Measured integrated jet shapes in DIS. On the right-hand side, calculations from the leading-logarithm parton-shower Monte Carlo LEPTO are shown for comparison.

quarks (upper curve), it is observed that the data go from being dominated by quarks to being dominated by gluons as η^{jet} increases. Thus, the broadening of the jets is consistent with an increasing fraction of gluon-initiated jets as η^{jet} increases.

6 Deep inelastic scattering at HERA

Two processes contribute to the dijet cross section in neutral-current DIS at LO in pQCD, namely the QCD Compton ($\gamma^* q \to qg$) and the Boson Gluon Fusion (BGF) ($\gamma^* g \to q\bar{q}$) processes. The cross section for jet production is given by

$$\sigma_{DIS} = \int d\Omega \; f_{j/p}(x_p, \mu_F^2) \; d\sigma_{\gamma^* j \to \text{jet jet}}(x_p \cdot P, \alpha_s(\mu_R^2), \mu_R^2, \mu_F^2), \tag{5}$$

where $f_{j/p}(x_p, \mu_F^2)$ are the parton densities in the proton and $d\sigma_{\gamma^* j \to \text{jet jet}}$ is the subprocess cross section. In the kinematic regimem studied, the BGF process represents the largest contribution and therefore the final state is expected to be dominated by quark-initiated jets.

7 Jet shapes in DIS

The integrated jet shape has been measured[18] using the 1994 H1[19] data ($\mathcal{L} \sim 2$ pb^{-1}) for dijet events in the Breit frame. The jets have been searched for with the iterative cone and the k_T cluster algorithms. The two jets with highest $E^{jet}_{T,\text{Breit}}$ (transverse with respect to the direction of the virtual photon in the Breit frame) which satisfy $E^{jet}_{T,\text{Breit}} > 5$ GeV and $-1 < \eta^{jet}_{\text{LAB}} < 2$ have been selected. The measurements are presented for different regions of $\eta^{jet}_{\text{Breit}}$ and $E^{jet}_{T,\text{Breit}}$ in the kinematic region given by $10 < Q^2 \lesssim 120$ GeV^2 and $2 \cdot 10^{-4} \lesssim x_{Bj} \lesssim 8 \cdot 10^{-3}$, where x_{Bj} is the Bjorken x variable.

Figure 4 shows the measured integrated jet shape as a function of r in different regions of $\eta^{jet}_{\text{Breit}}$ and two regions of $E^{jet}_{T,\text{Breit}}$ for the two jet algorithms. The data show that the jets get narrower as $E^{jet}_{T,\text{Breit}}$ increases and that the jets get broader as $\eta^{jet}_{\text{Breit}}$ increases (i.e. towards the proton direction). The broadening of the jets is more evident at low $E^{jet}_{T,\text{Breit}}$. At low $E^{jet}_{T,\text{Breit}}$, the jets defined by the k_T cluster algorithm are narrower than those defined by the iterative cone algorithm. At high $E^{jet}_{T,\text{Breit}}$ both algorithms produce very similar jets.

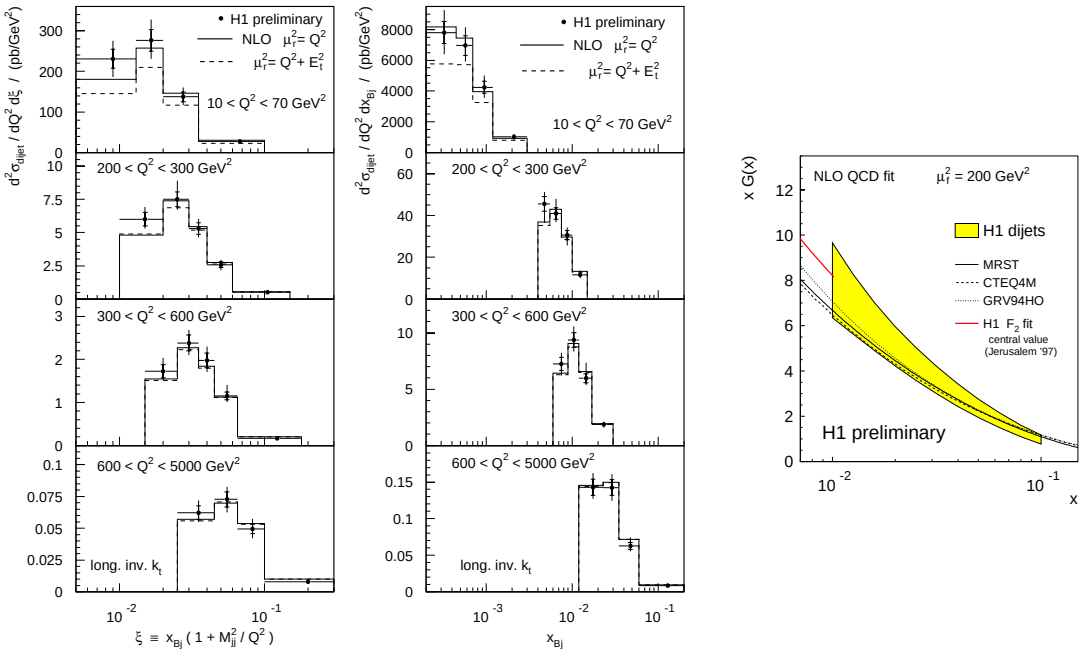

Figure 5: Measured dijet cross sections $d^2\sigma/dQ^2 d\xi$ and $d^2\sigma/dQ^2 dx_{Bj}$ in DIS (left-hand side). NLO QCD calculations are shown for comparison. On the right-hand side, the extracted gluon density in the proton is shown.

The QCD based MC LEPTO [20] predicts that gluon jets (dotted line in the right-hand side of figure 4) are broader than quark jets (dashed line) and that in the kinematic region of the measurements, the dijet sample is dominated by BGF and therefore by $q\bar{q}$ pairs in the final state. The comparison of the model predictions to the data shows that the measured jet shape is compatible with that of quark-initiated jets.

8 Dijet cross sections in DIS

Dijet cross sections in neutral-current DIS have been measured [21] using the 1994 – 1997 H1 data ($\mathcal{L} \sim 36$ pb^{-1}). The jets are defined by the k_T cluster algorithm in the Breit frame. The two jets with highest E_T^{jet} are required to have $E_{T,\mathrm{Breit}}^{jet} > 5$ GeV, $E_{T,\mathrm{Breit}}^{jet1} + E_{T,\mathrm{Breit}}^{jet2} > 17$ GeV and $-1 < \eta_{\mathrm{LAB}}^{jet} < 2.5$. The measurements of $d^2\sigma/dQ^2 d\xi$, where $\xi = x_{Bj}(1 + M_{JJ}^2/Q^2)$, and $d^2\sigma/dQ^2 dx_{Bj}$ are presented for the kinematic region given by $10 < Q^2 < 5000$ GeV^2 and $0.2 < y < 0.6$. The data have been corrected for detector effects, and for initial- and final-state QED radiation effects.

For the inclusive k_T cluster algorithm, the hadronisation effects are small and independent of Q^2. Thus, the data have been compared to the NLO calculations performed using the program DISENT [22].

The left-hand side of figure 5 shows the measured dijet cross sections in DIS as a function of ξ and x_{Bj} in different regions of Q^2 (black dots). The histograms are the NLO calculations from DISENT for two choices of the renormalisation scale: $\mu_R^2 = Q^2$ (solid histograms) and $\mu_R^2 = Q^2 + E_T^2$ (dashed histograms). The calculations based on different choices of μ_R^2 differ only at low Q^2. The dependence of the calculations on the factorisation scale is small. The NLO predictions give a reasonable description of the data at all values of Q^2 for the choice $\mu_R^2 = Q^2$.

9 Extraction of the gluon density in the proton

A direct determination [21] of the gluon density has been performed via a NLO QCD fit to the measured dijet cross sections. Inclusive neutral-current DIS data [23] have been used to constrain the quark densities. The determination of the gluon density has been done using the dijet cross sections for $Q^2 > 200$ GeV^2, where the hadronisation corrections are small and independent of Q^2, ξ and x_{Bj}. The theoretical uncertainties are also small in this kinematic region. The value for the strong coupling constant has been taken from the world average, $\alpha_s(M_Z^2) = 0.119 \pm 0.005$. The parton densities have been extracted at a factorisation scale $\mu_F^2 = 200$ GeV^2 in the range $0.01 < x < 0.1$.
The resulting quark densities are 5% higher at $x = 0.01$ than the results from global fits and they are in agreement at $x = 0.1$. The resulting gluon density together with its uncertainties is shown as a shaded band in the right-hand side of figure 5. This result is slightly higher than those from the global analyses, although compatible within the errors. It is in good agreement with the determination of the gluon density from the QCD analysis [24] of F_2 data at $x = 0.01$ (dark solid line) by the H1 Collaboration.

10 Summary and conclusions

Measurements of high-E_T inclusive jet and dijet cross sections in photoproduction have been presented. NLO QCD calculations give a reasonable description of the measured cross sections up to $E_T^{jet} \sim 74$ GeV. No significant deviation between data and calculations is observed up to dijet masses of $M^{JJ} \sim 140$ GeV.
The measurements of jet shapes in photoproduction and neutral-current DIS are consistent with the different parton contents of the final state expected in these two reactions: quark jets in DIS ($\gamma^* g \to q\bar{q}$ is the dominant subprocess), and an increasing fraction of gluon jets as η^{jet} increases in photoproduction (the resolved subprocess $q_\gamma g_p \to qg$ dominates over that of the direct $\gamma g \to q\bar{q}$ at large η^{jet}).
A direct determination of the gluon density in the proton has been made via a QCD fit to the dijet and inclusive neutral-current DIS data. The resulting gluon density is compatible within errors with the results from global analyses, supporting the universality of the gluon density.

Acknowledgments

I would like to thank the organisers for a very warm atmosphere and a well organised conference. Special thanks to my colleagues from H1 and ZEUS for their help in preparing this work. The work of the author is supported by an European Community fellowship under contract ERBFMBICT 972523.

References

1. C.F.v. Weizsäcker, *Z. Phys.* **88** (1934) 612; E.J. Williams, *Phys. Rev.* **45** (1934) 729.
2. A.D. Martin, R.G Roberts, W.J. Stirling, R.S. Thorne, hep-ph/9805205; M. Gluck, E. Reya, A. Vogt, *Z. Phys.* C **67** (1995) 433; CTEQ Collab., H.L. Lai *et al*, hep-ph/9903282.
3. ZEUS Collab., J. Breitweg *et al*, *Eur. Phys. Jour.* C **4** (1998) 591.
4. H1 Collab., T. Ahmed *et al*, *Nucl. Phys.* B **445** (1995) 195 and S. Aid *et al*, *Z. Phys.* C **70** (1996) 17
5. CDF Collab., F. Abe *et al*, *Phys. Rev.* D **45** (1992) 1448.
6. J. Huth *et al*, Proceedings of the 1990 DPF Summer Study on High Energy Physics, Snowmass, Colorado, edited by E.L. Berger (World Scientific, Singapore,1992) p. 134.

7. S. Catani, Yu.L. Dokshitzer, M.H. Seymour and B.R. Webber, *Nucl. Phys.* B **406** (1993) 187; S.D. Ellis and D.E. Soper, *Phys. Rev.* D **48** (1993) 3160; M.H. Seymour, *Nucl. Phys.* B **513** (1998) 269.
8. ZEUS Collab., Contributed paper to ICHEP'98, Vancouver, July 1998, N-812.
9. The ZEUS Detector, Status Report (1993), DESY 1993.
10. M. Klasen and G. Kramer, *Z. Phys.* C **76** (1997) 67; M. Klasen, T. Kleinwort and G. Kramer, DESY 97-234 (hep-ph/9712256).
11. B.W. Harris and J.F. Owens, *Phys. Rev.* D **56** (1997) 4007 and *Phys. Rev.* D **57** (1998) 5555.
12. L.E. Gordon and J.K. Storrow, *Nucl. Phys.* B **489** (1997) 405.
13. M. Glück, E. Reya and A. Vogt *Phys. Rev.* D **46** (1992) 1973.
14. P. Aurenche, J.P. Guillet, M. Fontannaz, *Z. Phys.* C **64** (1994) 621.
15. H.L. Lai *et al*, *Phys. Rev.* D **55** (1997) 1280.
16. ZEUS Collab., Contributed paper to ICHEP'98, Vancouver, July 1998, N-805.
17. H.-U. Bengtsson and T. Sjöstrand, *Comp. Phys. Comm.* **46** (1987) 43; T. Sjöstrand, *Comp. Phys. Comm.* **82** (1994) 74.
18. H1 Collab., C. Adloff *et al*, DESY 98-210 (December 1998).
19. H1 Collab., I. Abt *et al*, *Nucl. Instr. and Meth.* A **386** (1997) 310 and *Nucl. Instr. and Meth.* A **386** (1997) 348.
20. G. Ingelman, A. Edin and J. Rathsman, *Comp. Phys. Comm.* **101** (1997) 108.
21. H1 Collab., Contributed paper to ICHEP'98, Vancouver, July 1998, N-520.
22. S. Catani and M.H. Seymour, *Nucl. Phys.* B **485** (1997) 291; Erratum-ibid, *Nucl. Phys.* B **510** (1997) 503;
23. H1 Collab., Contributed paper to ICHEP'98, Vancouver, July 1998, N-533.
24. H1 Collab., Contributed paper to IECHEP'97, Jerusalem, August 1997, N-260.